Trends in Biomaterials and Artificial Organs
sbaoi
Original Article
www.sbaoi.org/tibao

Effect of Laser Peening on the Residual Stress Distribution and Wettability Characteristics of Ti-6Al-4V Alloy for Biomedical Applications

K. Praveenkumar[1], Geetha Manivasagam[1,2], S. Swaroop[3*]

[1]*School of Mechanical Engineering,* [2]*Centre for Biomaterials, Cellular and Molecular Theranostics,* [3]*Surface Modification Laboratory, School of Advanced Sciences, Vellore Institute of Technology, Vellore 632014, Tamil Nadu, India*

Received: *8 February 2021*
Accepted: *13 August 2021*
Published online: *23 February 2022*

Keywords: *Ti-6Al-4V, laser peening, compressive residual stress, wettability, micro-hardness*

In the present study, the effect of Laser Shock Peening without Coating (LPwC) on the surface and subsurface characteristics (i.e. residual stress, hardness in-depth direction, surface roughness, XRD and contact angle studies) of a Ti-6Al-4V alloy in the solution treated (ST) condition is considered. ST was carried out at 925ºC for 1 h, followed by air cooling. LPwC was performed using an Nd:YAG with 1064 nm wavelength, at three different power densities of 3, 6 and 9 GWcm^{-2} with fixed overlapping of 70%. The effect of LPwC was analysed using near-surface micrographs, residual stress distribution, surface roughness, X-ray diffraction, microhardness and surface contact angle studies. From the obtained results, it was concluded that the sample peened at 6 GW cm^{-2} was most suited for biomedical applications.

Introduction

Metallic implants are extensively used in biomedical applications where high strength are required. Traditional biomedical implant materials, such as titanium and its alloys [1–3], stainless steel, and partially stabilized zirconia are bio-inert. Specifically, Ti-6Al-4V is a workhorse in both surgical implants and the aviation sector due to a combination of good mechanical properties, high strength and low density [4,5]. Also, because its elastic modulus (110 GPa) and yield strength (840 MPa) are close to those of human bones, this avoids the stress shielding effect.

However, Ti alloys have moderate fatigue strength, wear and corrosion resistance. Rapid wear can lead to the degradation of mechanical properties that will adversely affect the recovery process. At the same time, wear scars will accelerate the rate of fatigue crack initiation and propagation. These wear scars act as pits and accelerate the corrosion process and therefore increase the corrosion products release rate. Wear debris and rapid release of metallic ions can be a health hazard. To avoid these failures and further subsequence, the surface needs to be protected. There are several techniques to modify the surface such as shot peening (SP), laser shock peening (LSP) [6-10], ball burnishing (BB) [11], deep rolling [12] and ultrasonic shot peening [13]. Among this laser shock peening is a relatively modern thermo-mechanical process. LSP uses a high energy laser pulse (few tens of nm FWHM (Full Width at Half Maximum) and several hundreds of mJ of energy) interacting with the material surface. This process generates a high amplitude shock wave through the rapid expansion of high-temperature plasma induced by laser irradiation. This laser deteriorated shock wave propagates into the metallic material leading to plastic deformation up to a certain depth. This leads to a work-hardening layer formed on the sample surface and sub-surface post-LPwC process. The effect of work-hardening causes an increase in strength and hardness of the material and decreases the ductility and toughness of materials [6,7]. Generally, the crack originates from the surface due to low toughness (brittle phase) during service, and mechanical inhomogeneity causes the raise in stress concentration under the external loading condition. LPwC delays the propagation of the surface cracks and hence increases the fatigue life.

In the present study, the as-received (AR) Ti-6Al-4V was subjected to laser shock peening without coating (LPwC) The effect of LPwC

* *Corresponding author*
sathyaswaroop.n.r@vit.ac.in (Dr. Sathya Swaroop, Surface Modification Laboratory, School of Advanced Sciences, Vellore Institute of Technology, Vellore 632014, Tamil Nadu, India)

on the surface micrographs, surface roughness, residual stress, microhardness, phase stability and wettability are discussed.

Materials and Methods

The material Ti-6Al-4V in the form of a bar of diameter 19 mm was obtained in the mill-annealed condition (ASTM B348). The chemical composition of the material was Al-6.16%, V-3.51%, Fe-0.117%, C-0.01%, other elements -0.149%, Ti balance (all in wt.%). Samples in the form of disks of a thickness of 5 mm were cut from the procured bar. The as-received (AR) samples were solution treated (ST) at 925 °C for 1 hr, followed by air cooling, to obtain a bimodal structure. The samples were then polished from #120 to #2500 grit using SiC (silicon carbide) polishing sheets and cleaned in ethanol before the process of laser peening.

Laser peening without coating (LPwC)

Laser shock peening without coating (LPwC) was performed using a pulsed Q-switched Nd:YAG laser (Litron lasers, UK) with a fundamental wavelength of 1064 nm and a pulse width of 10 ns. The laser beam was focused on the surface of the solution treated sample as a spot with a diameter of 0.8 mm, resulting in power densities of 3 (LP#3), 6 (LP#6) and 9 GW cm^{-2} (LP#9). The overlap between adjacent spots was maintained at 70%. There was no sacrificial coating, as the technique was LPwC. Running water with a thickness of ~ 1 mm was used as a confinement medium. A schematic of the LPwC process is shown in figure 1. During the LPwC process, a high-intensity laser beam penetrates through the transparent water confined medium and irradiates the target sample surface. This is ionized to form plasma confined by the water. Expansion of the plasma induces a shock wave into the target material, resulting in plastic deformation, work-hardening and compressive residual stress near the material surface and at the subsurface, thus improving the mechanical properties.

Microstructure

To study the microstructure, a cross-section of the sample subjected to LPwC specimen was polished as explained in section 2.1, followed by polishing with a 0.04 µm colloidal silica solution. For the grain boundaries to be revealed, samples were etched with Kroll's reagent containing 92% H_2O, 3% HNO_3 and 2% HF. The microstructure was characterized using an optical microscope (Carl-Zeiss A1 Mat Microscopy). The schematic of the heating cycle used for solution treatment is represented in figure 2. The microstructure of mill-annealed and solution treated samples were shown in figure 3. It should be noted that only solution treated samples were used for the LPwC process, as samples are normally used in solution treated conditions in typical biomedical applications.

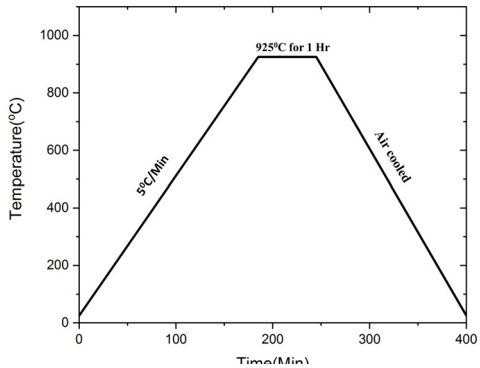

Figure 2: Heat treatment cycle for ST samples

Microhardness

Vickers microhardness (HV) of the unpeened and peened samples along their cross-section was measured with a hardness tester (Chennai Metco Pvt Ltd), to obtain the variation of microhardness along with the depth of the sample. The load used was 100 g and the holding time was 10 s. The average of three measurements at each depth was reported and the standard deviation was reported as an error bar.

Residual stress

The residual stress measurements of laser shock peened samples were carried out using XRD based $\sin^2\psi$ method (Proto LXRD, Canada). Residual stress measurement was performed with radiation of Cu-Kα with a primary aperture dimension of 1.5 mm x 5 mm. The peak selected in this study was (213) plane of the á phase corresponding to the Bragg angle (2θ) of 142°. The sample was tilted between -25 to +25°, relating to a total of 11 steps. The average residual stress was calculated from this by the slope of the d versus $\sin^2\psi$ plot using elastic modulus of 110 GPa and Poisson's ratio of 0.33.

Surface roughness

The surface roughness of the untreated and LPwCed samples was determined using contact mode (stylus) 2D-profilometer. The average roughness (R_a), maximum roughness (R_{max}) were measured in three different places of the samples and the average was reported.

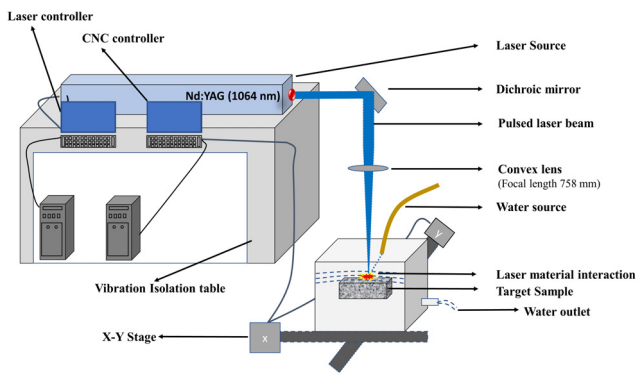

Figure 1: Schematic representation of LPwC process

Table 1. XRD parameters

X-ray source	Cu Kα
X-ray tube voltage	30 kV
X-ray tube current	40 mA
Incidence Beam angle	16°
2θ range	30-90°
Step size	0.02°
Step time	5 s

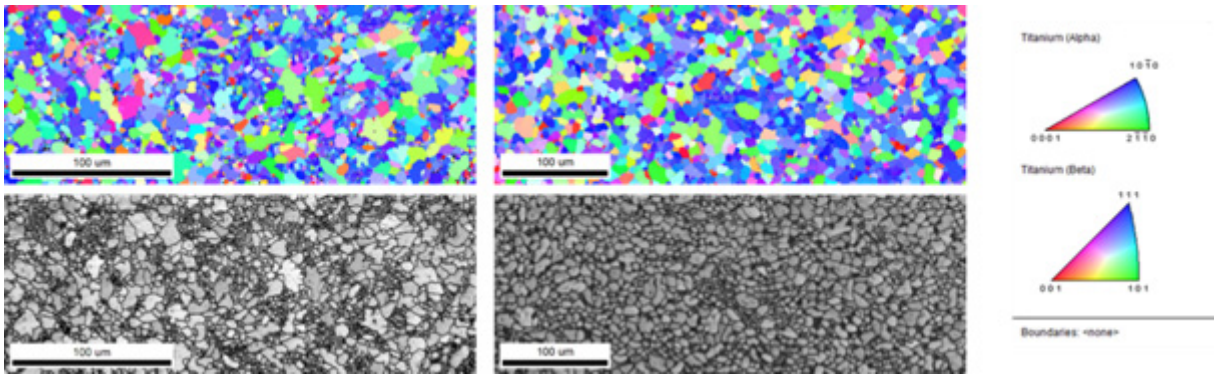

Figure 3: The microstructure of (a) As received, (b) Solution treated (925°C for 1hr followed by air-cooling)

X-ray diffraction

A high-resolution X-ray diffraction instrument (Brucker D8, USA) was used to investigate the peak broadening and phase transformation with characteristic CuKα_1 radiation (λ = 1.5406 Å) scanned from 30 to 90° at a step size of 0.02°. The XRD parameters are listed in table 1.

Surface wettability

Wettability was evaluated using water contact angle measurement performed by the sessile drop method. Static contact angle (CA) measurements using the droplet volume of 5 µl distilled water was used to examine the surface wettability characteristics using a goniometer system (Holmarc Opto-Mechatronics Pvt. Ltd.) at room temperature (25°C).

Electron backscatter diffraction (EBSD)

The as-received and solution treated samples were cut through depth direction using a low-speed diamond cutter (Model: Baincut, Make: Chennai metco Pvt Ltd.,) with coolant (Isomet oil as coolant). Further, the materials were polished the same way as described in section 2.1 and followed by electropolishing using Lectropol 5 (M/s Struers). The near-surface region in the cross-section of as-received and solution treated samples were analysed using Quanta 3D FEG (OIM lab at IIT Bombay) with an accelerating voltage of 20 kV. The scanned area of 300 µm * 300 µm with a step size of 0.4 µm were considered in this study.

Results and Discussion

Micro-Hardness and FWHM

Figure 4 shows the in-depth micro-hardness ($HV_{0.1}$) and figure 5 shows the FWHM depth distributions of the sample after the LPwC process. The surface hardness of the untreated sample was 340.21 $HV_{0.1}$ (unpeened). After the LPwC process, the highest hardness was observed at the surface (near-surface) for all conditions. LP#6 sample measured the highest magnitude of 527.3±15.13 $HV_{0.1}$ at the surface which is almost 1.55 times increase in the magnitude, in comparison with the unpeened sample. Under a similar comparable condition in an earlier study in the literature, Ti-6Al-4V induced around 330 to 375 HV which is lower than the present investigation [12]. The increase in the surface hardness did not monotonically increase with the increase in power density. The surface hardness of LP#9 dropped even below the LP#3 samples, indicating that it was not necessary to increase the power density beyond 6 GW cm^{-2} to derive the benefits of LPwC. This phenomenon was well recorded and discussed based on concurrent softening processes dominating over the hardening processes beyond a power density in an earlier investigation from our group [14–16]. The hardness reached the unpeened hardness level at a

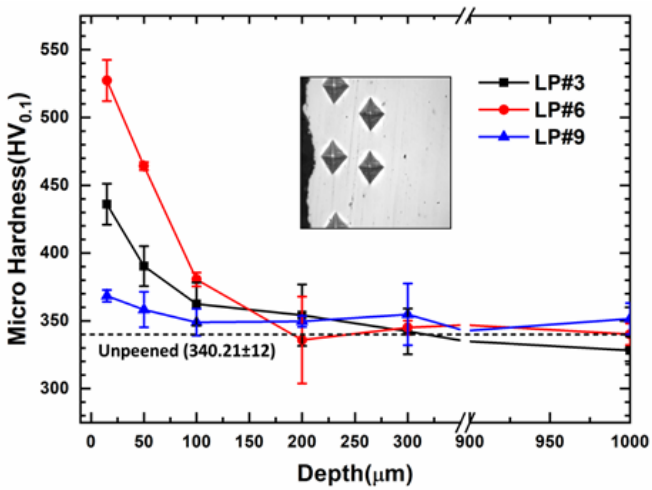

Figure 4: Microhardness distribution of LPwC samples

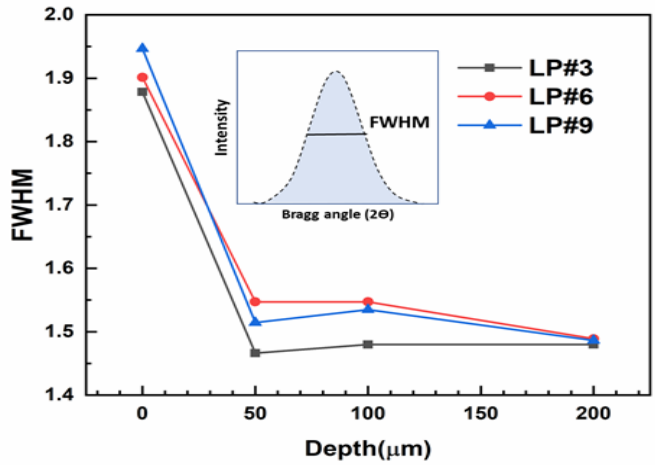

Figure 5: Comparison of FWHM of LP#3, LP#6 and LP#9 samples at <213> plane

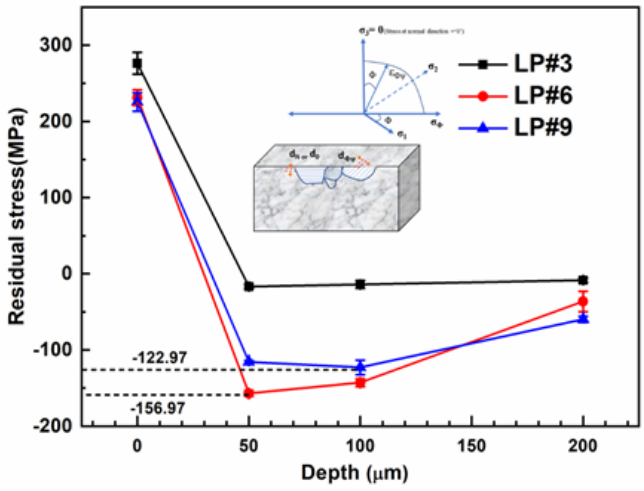

Figure 6: Residual stress distribution of LPwC samples

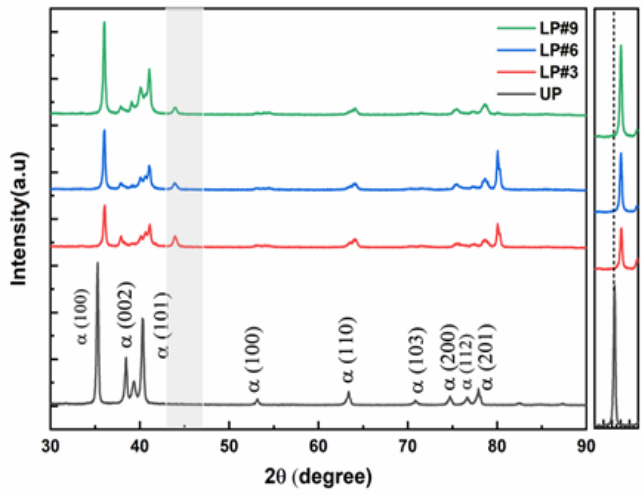

Figure 7: Surface XRD profile of LPwC samples

depth of 200 μm, roughly providing the estimate of work-hardened depth. This was due to the attenuation of a shock wave propagating into the material.

Generally, after the LPwC process, material hardness is accompanied by changes in the dislocation density that can be deduced by the FWHM of XRD peaks. The depth profile of FWHM (full width at half maximum) for Bragg peak of 142° at {213} plane are shown in figure 5. For all the LPwC processed samples the defect (dislocation) density is maximum at the surface and then slowly decreases and merges at 200 ìm from the surface. Although it was observed that LP#9 showed the least surface hardness, it still retained the highest defect density, indicating that the decrease in hardness could be due to additional factors such as thermal and microstructural effects at and near the surface.

Residual stress

Residual stress as a function of depth is represented in figure 6. It is observed that the tensile residual stress (TRS) of 276.34, 231.35 and 225.59 MPa for LP#3, LP#6 and LP#9 samples induced on the surface of the LPwC treated Ti-6Al-4V alloy. Similar results were observed in the investigation of the LPwC process on Inconel 718 alloy by Gill et al [17]. In our group Karthik et al., also observed the surface tensile residual stress on the surface of the AISI 321 steel post-LPwC process[18]. This could be due to the direct interaction of the laser beam with the material surface with the absence of absorbent coating, resulting in probable melting and re-solidification of the surface. In such a scenario, a rough surface would result. This was confirmed from the waviness of the roughness profiles. Below the surface, tensile residual stress(TRS) changes to compressive residual stress CRS, reached a maximum of -11, -156.97 MPa for LP#3 and LP#6 at 50 μm and -122.97 MPa for LP#9 samples at 100 μm. Beyond these maxima, there was a reversal from CRS to TRS and the compressive stress zone endured till approximately 200 μm. It should be noted that in the residual stress profile, increasing the power density beyond 6 GW cm^{-2} did not result in any further improvement, consistent with the discussion on the hardness profile, indicating some similarity in mechanisms of hardness and CRS improvement.

The X-Ray diffraction (XRD) patterns of Ti-6Al-4V alloy before and after LSP are illustrated in figure 7. It can be observed that both the unpeened and the LPwC samples have the same alpha peaks. However, the LPwC sample showed a new peak at a Bragg angle (2θ) around 43.95°. The peak was identified as TiO as per the JCPDS data (Card No. 85-2084). TiO is an unstable form of titanium oxide and its formation is aided by high pressure and temperature. As the pressure and temperature are both high during LPwC and

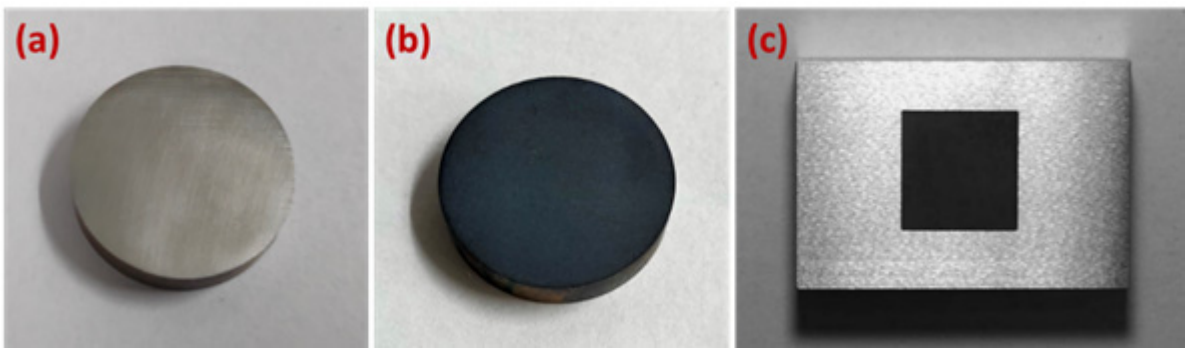

Figure 8: (a) unpeened, (b) LP#6 sample and (c) SUS304 plate laser peened on the centre (greyish) (Reprinted with permission from Elsevier) [19]

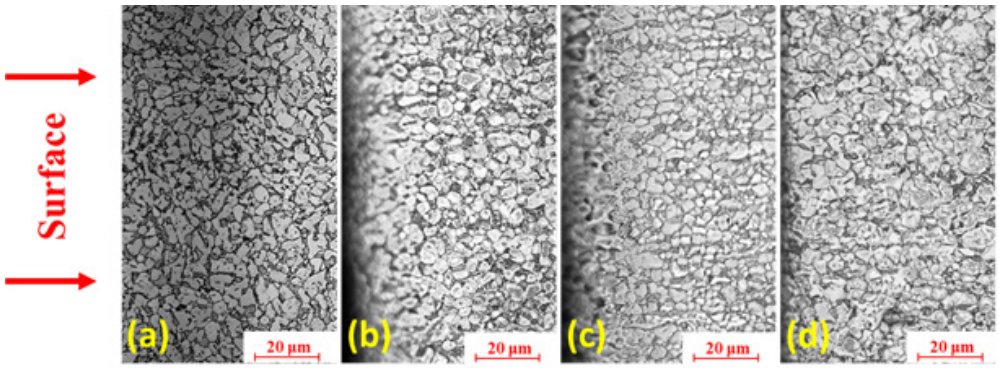

Figure 9: Crossectional micrographs of (a) unpeened, (b) LP#3, (c) LP#6 and (d) LP#9 samples

Table 2: Variation of crystallite size and crystal lattice strain of LPwC samples

Sample	Crystallite size (nm)	Crystal Lattice Strain
UP	52.0281	0.0010
LP#3	38.0909	0.0025
LP#6	26.5604	0.0028
LP#9	28.2759	0.0028

as indicated in the previous sections, it is reasonable to conclude that TiO could have formed during LPwC. The surface colour changed from silver to black, as shown in figure 8. The formation of oxides during peening is not uncommon and has been reported in other materials in the literature. For example, Sano et.al observed a change in colour of SUS 304 steel from silver to grey due to the formation of Cr_2O_3 on the surface [19].

Peak broadening and peak shifting were observed on the laser peened samples. It was evident from FWHM data. Peak broadening could be the result of variation in particle size as evaluated from Scherrer's equation, $D = \kappa\lambda/\beta\cos\theta$, where κ is constant (0.9), λ is the X-ray wavelength (1.54 nm), β is the FWHM and θ is the peak position. The broadening that occurs due to micro deformations would be a consequence of non-uniform strain and this value of microstrain (also termed as crystal lattice strain (ε)) can be calculated using the equation $\varepsilon = \beta/4\tan\theta$.

From table 2 it can be inferred that the LPwC process alters the crystalline size and microstrain on the samples. Crystallite size was decreased from 52 nm (unpeened) to 38.0909 nm, 26.5604 nm and 28.2759 nm for LP#3, LP#6 and LP#9 samples respectively. The lattice strain of the unpeened sample was 0.001 and for the LPwC sample, it is almost doubled in all the peening condition. This increase in crystal lattice strain is attributed to the cold working effect during the laser peening process. Based on these results, among the LPwCed samples, the sample peened at 6 GW cm^{-2} was

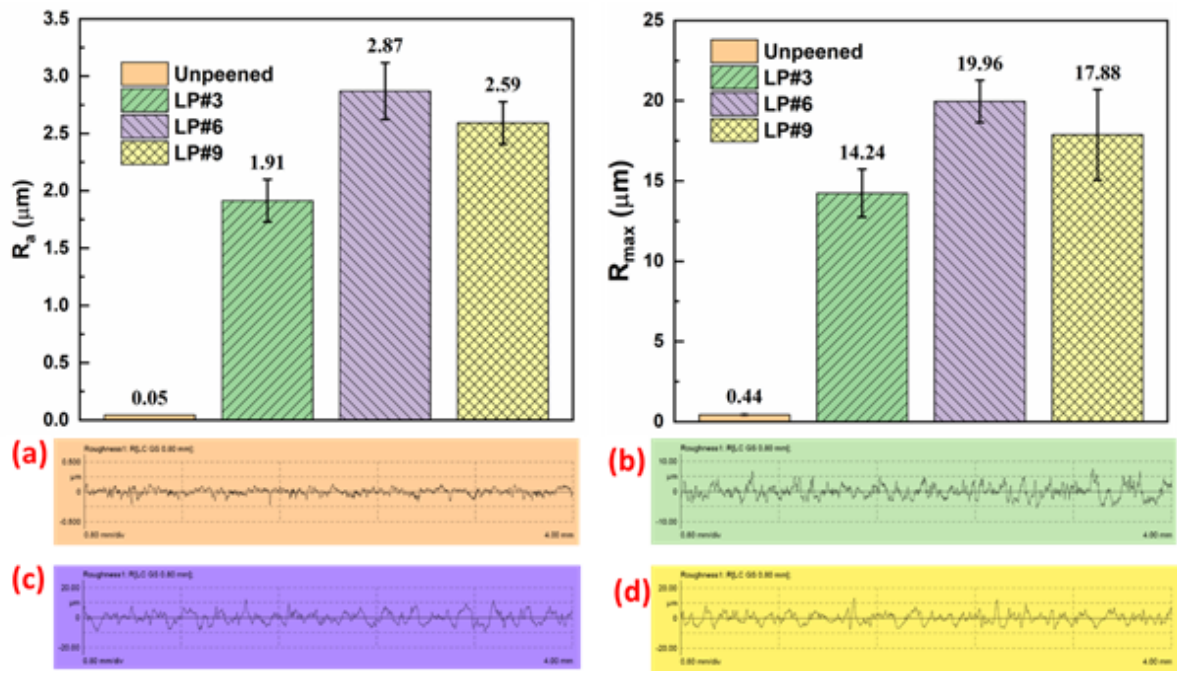

Figure 10: Surface roughness (2-D) of LPwC samples

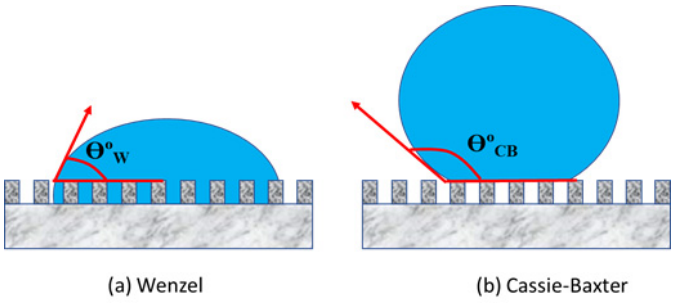

Figure 11: (a) Wenzel and (b) Cassie-Baxter model

found to be optimum for biomedical applications as also indicated earlier based on residual stress and hardness data.

The cross-sectional microstructure of LPwC sample:

Figure 9 compares the cross-section micrographs of Ti-6Al-4V alloy before and after LPwC treatment. Figure 9 (a) shows the unpeened, and (b), (c) and (d) represents the LPwC processed samples. Post-laser peening showed no dislocations (such as twins) or secondary phase (such as lamellar structure) observed from the optical micrographs. The average grain size (calculated based on line intercept method) of unpeened samples was around 5.625 ìm and after the LPwC process samples grain size decrease to ~3 ìm for all the peened samples. However, advanced techniques such as EBSD analysis need to be performed to know the detailed grain refinement study. The affected depth of LPwC is approximately 250 ìm from the surface. From this, it could be concluded that grain refinement near the surface resulted in the surface strengthening of the material, in addition to beneficial residual stress distribution.

Surface Roughness:

Fatigue and bio-implant performance are highly dependent on the surface finish; hence it needed to be studied. Figure 10 shows the surface roughness (R_a and R_{max}) of untreated and LPwC treated samples. It was observed that the unpeened sample showed a relatively smooth surface (R_a=0.05 ìm and R_{max} = 0.44 µm) than the LPwC samples. It was because the unpeened samples were polished before the test using colloidal silica to obtain a mirror finish. Moreover, the laser peened sample showed relatively high roughness. LP#3, LP#6 and LP#9 samples showed the average roughness of 1.91, 2.87 and 2.59 ìm respectively. Among these, LP#6 showed the relatively highest roughness. The difference in average roughness (R_a) values was due to the difference in the levels of heat input at the surface as a function of power density, especially in the absence of absorbent coating. Maximum roughness (R_{max}) was also higher for LP#6 sample of around 19.96 µm whereas LP#3 and LP#9 showed the R_{max} of 14.24 and 17.88 µm. This increase in roughness elevates the contact angle. It should be noted that the largest surface roughness of the LP#6 sample was compensated by the better residual stress and hardness profiles. Therefore, optimization of LPwC parameters needs to be carried out based on a combination of residual stress, hardness and roughness profiles. When all parameters were considered, LP#6 was found to be favourable for the chosen application.

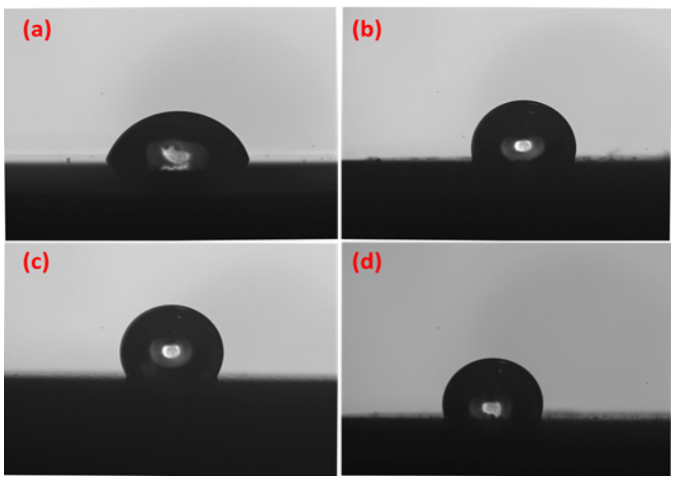

Figure 12: Contact angle images of (a) unpeened, (b) LP#3, (c)LP#6 and (d)LP#9 samples

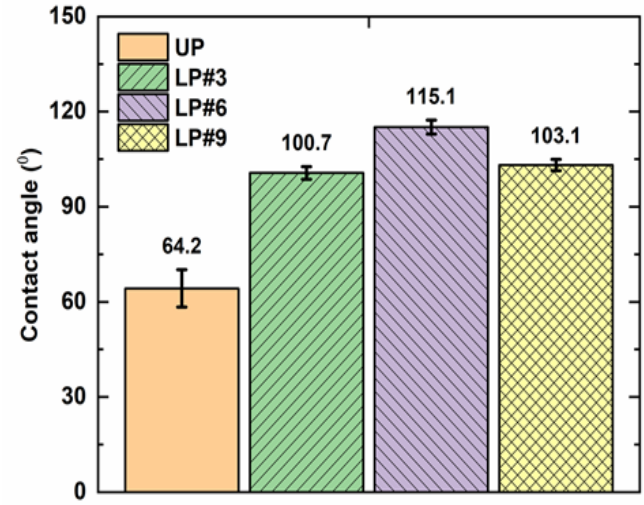

Figure 13: Water contact angle (°) of LPwC samples

Water Contact angle Studies:

Contact angle (CA) measurement is a useful and commonly used surface characterization method to study wettability. The CA between a liquid and a solid is the angle within the body of the liquid formed at the gas-liquid-solid interface. Depending upon the physical properties of the material surface CA can be large or small. Generally, the CA>90° results in hydrophobicity (low wettability), while CA<90° is considered as hydrophilicity (high wettability)[20]. From the surface roughness it was observed that post-LPwC process surface roughness increased. This change in the roughness values can alter the wettability characteristics of the LPwC samples. There are two classical models based on which the solid surface wetting occurs - Wenzel and Cassie–Baxter models [21,22]. Figure 11(a) shows, If the water drop (liquid) completely occupies the space between the valleys of the rough surface then the CA (θ) is described by Wenzel's equation. In another case, the air is entrapped under the fluid and the liquid at that point sits on a superficial level. In such a case the liquid contact with the solid surface is extraordinarily lessened and the system is represented by the Cassie–Baxter condition, which is shown in figure 11(b).

In the present study, CA of Ti-6Al-4V alloy before and after LPwC

Process wetted with distilled water and the contact angle is presented in figures 12 and 13. The CA of the unpeened specimen was measured to be hydrophilic (64.2º) in nature. However, post LPwC process, sample surface change from hydrophilic to hydrophobic for the all-peened condition. The values are 100.7º, 115.1º and 103.1º for LP#3, LP#6 and LP#9 conditions respectively This may be due to the change in surface morphology and surface energy. Earlier studies found, CA decrease with an increase in surface roughness[22]. However, in the case of LPwC treated samples it was observed that an increase in contact angle was due to the change in surface roughness. B. S. Yilbas et al observed a water contact angle of 44.8º in Ti-6Al-4V before peening and post-laser peening, the surface contact angle increased to 85.2º which is lower than the present study [23]. The high roughness observed in section 3.5 might cause an increase in the contact angle. This unevenness is formed on the surface during the LPwC process due to laser and material-interaction in presence of water. This roughness alters the surface free energy and increases the contact angle [24]. Also, peening removes the surface impurities (such as dirt, foreign objects). All together increases the high contact angle (hydrophobic), thus resisting corrosion by repelling water molecule.

Conclusion

LPwC was carried out on a Ti-6Al-4V alloy using a power density of 3, 6 and 9 GW cm^{-2} with a fixed overlapping rate of 70% and the following conclusions could be drawn. Work-hardening was observed on all LPwC samples. However, beyond 6 GW cm^{-2}, there was a saturation of the benefits of LPwC. This was confirmed by measurements of micro-hardness, FWHM and residual stress studies. The maximum residual stress was found to be -156.97 MPa for 6 GW cm^{-2} samples. There was no phase change post-LPwC process. However, peak broadening and peak shifting was observed. The presence of TiO phase was observed at the Bragg angle of 43.95º for the peened sample. The average surface roughness of the peened samples were found to be < 3 µm. After the LPwC process, the unpeened hydrophilic sample surface (64.2º) improved to hydrophobic surface 100.7º,115.7º and 103.1º for LP#3, LP#6 and LP#9 samples.

Acknowledgement

We thank AR&DB, India (Grant No. ARDB/GTMAP/01/2031839/M/I) for the financial support, Vellore Institute of Technology, Vellore for the infrastructure and constant support throughout the project and Dr Phani Mylavarapu (DMRL, Hyderabad) for the residual stress measurements.

References

1. D. Gopi, E. Shinyjoy, A. Karthika, S. Nithiya, L. Kavitha, D. Rajeswari, T. Tang, Single walled carbon nanotubes reinforced mineralized hydroxyapatite composite coatings on titanium for improved biocompatible implant applications, RSC Advances. 5, 36766–36778 (2015).
2. A. Karthika, L. Kavitha, M. Surendiran, S. Kannan, D. Gopi, Fabrication of divalent ion substituted hydroxyapatite/gelatin nanocomposite coating on electron beam treated titanium: Mechanical, anticorrosive, antibacterial and bioactive evaluations, RSC Advances. 5, 47341–47352 (2015).
3. D. Gopi, S. Nithiya, E. Shinyjoy, D. Rajeswari, L. Kavitha, Carbon nanotubes/carboxymethyl chitosan/mineralized hydroxyapatite composite coating on Ti-6Al-4V alloy for improved mechanical and biological properties, Industrial and Engineering Chemistry Research. 53, 7660–7669 (2014).
4. I. Gurappa, Characterization of different materials for corrosion resistance under simulated body fluid conditions, Materials Characterization. 49, 73–79 (2002).
5. R.R. Boyer, An overview on the use of titanium in the aerospace industry, Materials Science and Engineering A. 213, 103–114 (1996).
6. C.S. Montross, T. Wei, L. Ye, G. Clark, Y.W. Mai, Laser shock processing and its effects on microstructure and properties of metal alloys: A review, International Journal of Fatigue. 24, 1021–1036 (2002).
7. A.K. Gujba, M. Medraj, Laser peening process and its impact on materials properties in comparison with shot peening and ultrasonic impact peening, Materials (Basel), 7(12), 7925-7974 (2014).
8. B. Dhakal, S. Swaroop, Review/ : Laser shock peening as post welding treatment technique, Journal of Manufacturing Processes. 32, 721–733 (2018).
9. S.S. Rajan, S. Swaroop, G. Manivasagam, M.N. Rao, Fatigue Life Enhancement of Titanium Alloy by the Development of Nano/Micron Surface Layer Using Laser Peening, Journal of Nanoscience and Nanotechnology. 19, 7064–7073 (2019).
10. B. Jose, T. Patil, S. Sudhagara Rajan, K. Praveenkumar, G. Manivasagam, S. Swaroop, Effect of laser shock peening without coating (LPwC) on a surface and sub-surface characteristics of aged Ti 15/ V-3Al- 3Cr-3Sn alloy, Materials Today: Proceedings. (2021).
11. M. Abdulstaar, M. Mhaede, M. Wollmann, L. Wagner, Investigating the effects of bulk and surface severe plastic deformation on the fatigue, corrosion behaviour and corrosion fatigue of AA5083, Surface and Coatings Technology. 254, 244–251 (2014).
12. R.K. Nalla, I. Altenberger, U. Noster, G.Y. Liu, B. Scholtes, R.O. Ritchie, On the influence of mechanical surface treatments-deep rolling and laser shock peening-on the fatigue behavior of Ti-6Al-4V at ambient and elevated temperatures, Materials Science and Engineering A. 355, 216–230 (2013).
13. Y. zhang HE, D. po WANG, Y. WANG, H. ZHANG, Correction of buckling distortion by ultrasonic shot peening treatment for 5A06 aluminum alloy welded structure, Transactions of Nonferrous Metals Society of China (English Edition). 26, 1531–1537 (2016).
14. A. Umapathi, S. Swaroop, Residual stress distribution in a laser peened Ti-2.5Cu alloy, Surface and Coatings Technology. 307, 38–46 (2016).
15. A. Umapathi, S. Swaroop, Wavelength dependent deformation in a laser peened Ti-2.5Cu alloy, Materials Science and Engineering A. 684, 344–352 (2017).
16. A. Umapathi, S. Swaroop, Mechanical properties of a laser peened Ti-6Al-4V, Optics and Laser Technology. 119, 105568 (2019).
17. A.S. Gill, A. Telang, V.K. Vasudevan, Characteristics of surface layers formed on inconel 718 by laser shock peening with and without a protective coating, Journal of Materials Processing Technology. 225 (2015) 463–472. https://doi.org/10.1016/j.jmatprotec.2015.06.026.
18. D. Karthik, S. Swaroop, Laser peening without coating induced phase transformation and thermal relaxation of residual stresses in AISI 321 steel, Surface & Coatings Technology. 291, 161–171 (2016).
19. Y. Sano, M. Obata, T. Kubo, N. Mukai, M. Yoda, K. Masaki, Y. Ochi, Retardation of crack initiation and growth in austenitic stainless steels by laser peening without protective coating, Materials Science and Engineering A. 417, 334–340 (2006).
20. D. Patel, V.K. Jain, J. Ramkumar, Surface Texturing for Inducing Hydrophobicity, Directions, 15(1), 46–53 (2015).
21. L. Hao, J. Lawrence, Y.F. Phua, K.S. Chian, G.C. Lim, H.Y. Zheng, Enhanced human osteoblast cell adhesion and proliferation on 316 LS stainless steel by means of CO_2 laser surface treatment, Journal of Biomedical Materials Research Part B: Applied Biomaterials. 73B, 148–156 (2005).
22. S. Razi, K. Madanipour, M. Mollabashi, Improving the hydrophilicity of metallic surfaces by nanosecond pulsed laser surface modification, Journal of Laser Applications. 27, 42006 (2015).
23. B.S. Yilbas, H. Ali, A. Al-Sharafi, H. Al-Qahtani, Laser processing of Ti6Al4V alloy: wetting state of surface and environmental dust effects, Heliyon. 5(2), e01211 (2019).
24. V.K. Caralapatti, S. Narayanswamy, Analyzing the effect of high repetition laser shock peening on dynamic corrosion rate of magnesium, Optics and Laser Technology. 93, 165–174 (2017).